Research Square

Preprints are preliminary reports that have not undergone peer review.
They should not be considered conclusive, used to inform clinical practice,
or referenced by the media as validated information.

In vivo antitumor activity of dendritic cell-vaccinated skin flap model for mouse breast cancer

Yoshitaka Haga
Shizuoka Cancer Center
Yasuto Akiyama
Shizuoka Cancer Center
Tadashi Ashizawa
Shizuoka Cancer Center
Akari Kanematsu
Shizuoka Cancer Center
Chie Maeda
Shizuoka Cancer Center
Tomoatsu Ikeya
Shizuoka Cancer Center
Akira Iizuka
Shizuoka Cancer Center
Takashi Sugino
Shizuoka Cancer Center
Hiroki Mori
Institute of Science Tokyo
Jun Araki
ja980079@yahoo.co.jp

Shizuoka Cancer Center

Research Article

Keywords:

Posted Date: November 6th, 2026

DOI: https://doi.org/10.21203/rs.3.rs-8268574/v1

License: This work is licensed under a Creative Commons Attribution 4.0 International License. Read Full License

Additional Declarations: No competing interests reported.

Abstract

Despite advances in immune checkpoint inhibitor (ICI) therapy, managing locally advanced breast cancer remains a major challenge in clinical oncology. Our previous study introduced a dendritic cell (DC)-based skin-flap vaccination strategy using a rat model. The aim of this study was to establish a mouse immune-flap vaccination model targeting breast cancer and to evaluate its antitumor efficacy with or without ICI therapy. Mature DCs were generated from mouse bone marrow cells stimulated with tumor lysates and lipopolysaccharide. DC migration to regional lymph nodes was assessed 24 h after injection of labeled DCs into the skin flap using flow cytometry. In the DC vaccination experiment, immune cell subpopulations within tumors and antitumor effects were evaluated using flow cytometry and enzyme-linked immunospot assays after four weekly DC injections. Injected DCs successfully migrated to regional lymph nodes 24 h post-injection. Both the DC vaccine and anti-PD-1 antibody groups demonstrated potent antitumor effects *in vivo*, achieving over 50% tumor size reduction. However, the combination treatment exhibited a markedly weaker response. Tumor-infiltrating lymphocyte analysis demonstrated that the levels of $CD4^+$ memory T cells, macrophages, and B cells increased in the DC vaccine group, $CD8^+$ effector T cell levels increased in the anti-PD-1 antibody group, and tumor-infiltrating immune cell levels significantly decreased in the combination group. These findings highlight the potential of immune flap-based vaccination as a novel immunotherapeutic strategy. However, the diminished efficacy observed with combination therapy emphasizes the need to optimize treatment regimens.

Introduction

Recurrence following breast-conserving surgery in patients with locally advanced breast cancer remains a major clinical concern, necessitating the development of novel therapeutic approaches. In stage III or higher disease, the rate of local recurrence ranges from 30% to 50% [1, 2]. Therefore, postoperative adjuvant or neoadjuvant combination therapy is considered the standard treatment [3, 4]. This challenge is particularly pronounced in cases of advanced triple-negative breast cancers (TNBCs), where therapeutic options are severely limited because chemotherapy, often partly combined with immune checkpoint inhibitors (ICIs), remains the principal standard therapy [5, 6].

Recent clinical studies have explored the use of neoadjuvant chemotherapy combined with ICIs in several solid cancers, such as melanoma, non-small cell lung cancer, and breast cancer [7–11]. Notably, Schmid *et al.* demonstrated in the KEYNOTE-522 phase 3 clinical trial that patients with early-stage TNBC administered neoadjuvant pembrolizumab combined with chemotherapy achieved significantly higher pathological complete response rates and lower disease progression than those receiving placebo [10]. However, these findings apply primarily to early-stage TNBCs, and effective therapeutic regimens for advanced TNBC remain limited.

In a previous study, we introduced a novel dendritic cell (DC)-based immunotherapy using a rat model in which a DC-vaccinated skin flap was transplanted as an immunotherapeutic device [12]. This approach elicited tumor-specific immune responses and prevented local cancer recurrence *in vivo*.

Therefore, in the present study, we used an implanted skin flap to target local recurrence and residual breast cancer lesions (Fig. 1). To achieve this, we established a mouse immune-flap vaccination model using mouse breast cancer cells (EMT-6) [13, 14], and evaluated its antitumor efficacy with or without ICI therapy.

Materials and methods

Animals and cell lines

Seven- to nine-week-old female BALB/cA mice were purchased from CLEA Japan, Inc. (Tokyo, Japan). All procedures followed the Animal Research: Reporting In Vivo Experiments (ARRIVE) guidelines, which were originally developed in 2010 and updated in 2020 [15]. The mice were housed in plastic cages with ad libitum access to water and food, and maintained under controlled temperature (23 ± 2°C) and humidity (50% ± 20%). At the end of the experiments, all mice were euthanized using an isoflurane anesthesia system (Muromachi Kikai Co., LTD, Tokyo, Japan).

All experimental protocols were approved by the Animal Care and Use Committee of Shizuoka Cancer Center Research Institute. The mouse breast cancer cell line EMT6 (CRL-2755) was purchased from the American Type Culture Collection (Manassas, VA, USA).

Reagents and antibodies

Antibodies were used for DC characterization and tumor-infiltrating lymphocyte (TIL) analysis of mouse tumors using flow cytometry, as described previously [16]. For T-cell subsets, the antibodies used included anti-CD3-FITC (17A2), anti-CD4-PE (GK1.5), anti-CD8a-PerCP (53 – 6.7), anti-CD45-APC (30-F11), and anti-CD69-PE-Cy7 (H1.2F3). For naïve/effector/memory T-cell subsets, anti-CD44-FITC (IM7), anti-CD62L-PE-Cy7 (MEL-14), and anti-CD127-APC (A7R34) antibodies were used. For exhausted T-cell subsets, the antibodies included anti-CD279 (PD-1)-FITC (29F.1A12), anti-CD223 (LAG-3)-PE (C9B7W), anti-CD366 (TIM-3)-APC (B8.2C12), and anti-CD39-PE-Cy7 (Duha69). For natural killer (NK) and B cell subsets, the antibodies used were anti-B220-PE (RA3-6B2), anti-NK1.1-APC (PK136), and anti-CD19-PE-Cy7 (6D5). For myeloid-derived suppressor cells (MDSC) and macrophage subsets, the antibodies used included anti-mouse I-A/I-E-PE (MHC-class II, M5/114.15.2), anti-Ly-6G/Ly-6C (Gr-1)-PerCP (RB6-8C5), anti-CD11b-FITC (M1/70), anti-CD11c-FITC (N418), and anti-F4/80-PE-Cy7 (BM8). Antibodies used for the DC subset were anti-CD80-APC (16-10A1), anti-CD86-PerCP (GL-1), and anti-CD205-PE-Cy7 (NLDC-145). Finally, for the regulatory T cell subset, the antibodies used were anti-CD25-APC (3C7) and anti-GARP (LRRC32)-PE-Cy7 (F011-5). All antibodies were purchased from BioLegend, Inc. (San Diego, CA, USA). The anti-PD-1 antibody used for the *in vivo* experiments was purchased from Bio X Cell (Lebanon, NH, USA).

Production of bone marrow (BM)-derived DCs

BM-derived DC cultures and tumor cell lysates were generated as described previously [12, 17]. Briefly, unfractionated mouse BM cells were resuspended in Roswell Park Memorial Institute (RPMI) 1640 medium (Sigma-Aldrich, MO, USA) containing 2% fetal bovine serum (Biowest, Maine-et-Loire, France) and incubated with 10 ng/mL recombinant granulocyte-macrophage colony-stimulating factor (GM-CSF; PeproTech, Thermo Fisher Scientific, MA, USA) and 10 ng/mL recombinant interleukin-4 (PeproTech, Thermo Fisher Scientific, MA, USA) for 7 days. On day 7, DC-enriched cells were mixed with EMT6-derived tumor lysates and incubated for 24 h at 37°C in a CO_2 incubator. On day 8, lipopolysaccharide (LPS; *E. coli* K12-derived; InvivoGen, San Diego, CA, USA) was added to the culture medium and incubated for 24 h at 37°C. On day 9, mature DCs were collected, washed with serum-free RPMI 1640 medium, and injected subcutaneously into the mouse skin flap tissues. For DC-tracking experiments *in vivo*, lysate-treated mature BM-derived DCs were labeled with Deep Red immunofluorescence reagent (Abcam, Cambridge, UK) and used for subsequent experiments.

In vivo experiments using the EMT6 tumor model with skin flap transplantation

Two *in vivo* experiments were performed using female BALB/cA mice aged 7–9 weeks: DC tracking and DC vaccination. EMT6 tumor cells (2×10^5 cells/mouse) were transplanted subcutaneously into mice on day 14, and a skin flap was prepared on day 7 as described previously.[12] DC injections into the skin flap were initiated on day 0 (Supplemental Fig. 1).

In the DC tracking experiment, Deep Red-labeled DCs (1×10^6 cells/mouse) were injected once into the skin flap. After 24 and 48 h, lymph nodes from the skin flap were collected and a single-cell suspension was prepared. The Deep Red-positive DCs were analyzed using flow cytometry.

In the DC vaccination experiments, both short-term (administered twice, on days 0 and 7) and long-term (administered four times, on days 0, 7, 14, and 21) vaccinations were performed.

Four cohorts (n = 5/group) were established: control (physiological saline alone), DC vaccine alone, anti-PD-1 antibody alone, and a combination of the DC vaccine and anti-PD-1 antibody. Tumors and spleens were harvested on days 14 or 28 for the analysis of antitumor effects and immune responses using enzyme-linked immunospot (ELISPOT) assay, real-time PCR, and immunohistochemistry (IHC) analysis (Fig. 2a). Anti-PD-1 antibody was administered intraperitoneally at 2 mg/kg once weekly during DC vaccination, either alone or in combination with the DC vaccine. Tumor volume and body weight were measured twice weekly and tumor dimensions were measured using calipers. The tumor volume was calculated using the National Cancer Institute formula as follows: tumor volume (mm^3) = length (mm) × [width (mm)]^2 × 1/2.

Mouse immune cell-based ELISPOT assay

First, a 96-well microplate specific for the ELISPOT assay (ELISpot Flex: mouse IFN-γ-ALP, MABTEC Inc., Nacka Strand, Sweden) was precoated with anti-mouse IFN-γ antibody and incubated overnight. Subsequently, 2×10^5 mouse spleen cells were incubated with 2×10^3 irradiated EMT6 tumor cells (at a 100:1 E/T ratio) in each well overnight at 37°C. After removing the cells, mouse IFN-γ was stained with biotinylated IFN-γ detection antibody and streptavidin-ALP conjugates. Finally, the mouse IFN-γ-positive spots were measured using an AID ELISPOT reader (Autoimmun Diagnostika GmbH, Strassberg, Germany).

Immunohistochemistry

The following antibodies were used for immunohistochemical staining: anti-CD4 rabbit monoclonal antibody (D7D2Z), anti-CD8 XP rabbit monoclonal antibody (D4W2Z) (Cell Signaling Technology Inc., Danvers, MA, USA), anti-F4/80 rat monoclonal antibody (C1:A3-1; Cedarlane Laboratories, Ontario, Canada), and anti-FoxP3 rabbit monoclonal antibody (D6O8R; Cell Signaling Technology). Formalin-fixed paraffin-embedded cancer tissue blocks and sections were prepared from EMT6 mouse tumors and stained with various antibodies against immune cells. The number of positively stained cells in five high-magnification (×200) fields of view was calculated using the WinRoof image analysis software (Mitani Corporation, Tokyo, Japan) with an in-house algorithm, as described previously [18].

Real-time PCR analysis of mouse cytokines

Real-time PCR analysis of mouse cytokine/chemokine genes, including *CD3Z, CD4, CD8, CD16, CD19, CD39, CD68, CSF-1, CD83, CTLA4, FOXP3, CD274, CCL3, CCL4, CCL22, CCR4, CCR6, CCR7, CXCL10, CXCL12, CXCR3, ARG1, IL2, TNFA, IFNG, IL12A*, and *GZMB*, was performed using the QuantStudio 12 K Flex Real Time PCR System (Thermo Fisher Scientific, Waltham, MA, USA), as described previously [16]. Total RNA was isolated from mouse EMT6 tumor tissues using the High Pure RNA Paraffin Kit (Roche Diagnostics, Indianapolis, IN, USA).

Statistical analysis

Significant differences in tumor volume were analyzed using the Steel test (non-parametric) for multiple comparisons, whereas differences in immunological parameters were analyzed using the Mann–Whitney U test (non-parametric) or Student's t-test (parametric). Results with *P*-values < 0.05 were considered statistically significant.

Results

Characterization of mouse BM-derived DCs and tracking of labeled DCs in skin-flap lymph nodes

Treatment of immature DCs with tumor lysates and LPS induced a fully mature phenotype characterized by expression of markers such as CD11c, CD80, CD86, and MHC class II (Fig. 2b). When labeled with the Deep Red reagent, almost all DCs were positively stained and retained the expression of specific DC markers, including CD11c and MHC class II (Supplementary Fig. 2). In the single DC injection group, Deep Red-positive cells were distinctly observed within the skin flap lymph nodes (Supplementary Fig. 2; Table 1).

Table 1. Detection of DeepRed-positive DCs in skin flap-contained lymph nodes

Groups	$CD11c^+MHC\text{-}classII^+$ (%)	*P* value	$DeepRed^+MHC\text{-}classII^+$ (%)	*P* value
Control	14.6 ± 3.58	-	0	-
DC-treated	11.9 ± 2.68	0.40	2.69 ± 1.53	0.064

Each value represents the percentage of marker-positive cells, shown as the mean ± standard deviation of triplicate samples. Control: tumor inoculation only, DC-treated: tumor inoculation with DC injection, DC: dendritic cell. Statistical analysis was performed using the Mann–Whitney U-test. P-value vs. control group.

Effect of skin-flap-based DC vaccination on EMT6 tumor proliferation

In the short-term DC vaccination experiment, both DC and anti-PD-1 antibody-treated groups demonstrated a significant reduction in tumor size, exceeding 50%. However, the combination therapy group, which received both DC vaccination and anti-PD-1 antibody treatment, showed only a moderate antitumor response (Fig. 3a). In the long-term vaccination experiment, despite the continuation of treatment, the antitumor effect observed in the combination therapy and anti-PD-1 antibody groups tended to be attenuated compared to that in the DC-vaccinated group (Fig. 3b).

Characterization of tumor-specific CTLs from spleen cells using ELISPOT assay

The ELISPOT assay revealed that spleen cells from the DC vaccine-treated group produced higher levels of IFN-γ in response to EMT6 tumor cells than those from the saline-treated control group (Fig. 4). In contrast, the anti-PD-1 alone group showed few IFN-γ-positive spots. Moreover, elevated baseline levels of mouse IFN-γ were observed, even in splenocytes without EMT6 cell stimulation, suggesting that DC vaccination may induce a non-specific IFN-γ response.

Characterization of T-cell subpopulations in TILs and spleen cells via flow cytometry and immunohistochemistry

Flow cytometric analysis of TILs revealed that DC vaccination tended to increase the number of $CD4^+$ cells, particularly central memory T cells, whereas anti-PD-1 antibody treatment tended to increase the population of effector $CO8^+$ cells. In addition, both groups showed an increase in the $F4/80^+$ macrophage population (Tables 2 and 3). Complementary findings were observed in the IHC analysis of the TILs. However, DC vaccination tended to increase the number of $FoxP3^+$ cells, although this increase was not statistically significant. All the immune cell populations were reduced in the combination therapy group (Fig. 5).

Table 2
Flow cytometry analysis of tumor infiltrating lymphocytes from control and DC-vaccinated mice bearing EMT-6 tumors

	Cell populations	**Control**			**DC**				**DC/aPD-1 Ab**				**aPD-1 Ab**			
Separation data		Ave.		SD	Ave.		SD	*P* value	Ave.		SD	p value	Ave.		SD	*P* value
	Tumor weight (g)	0.22	±	0.12	0.12	±	0.03	0.280	0.28	±	0.07	0.549	0.14	±	0.03	0.376
	Collected cells ($\times 10^6$)	7.03	±	1.3	3.62	±	2.1	0.086	17.8	±	5.9	0.080	6.78	±	0.9	0.801
	CD45+/Total living cells (%)	48	±	7.8	53.5	±	8.4	0.456	36.9	±	6.8	0.135	41.2	±	3.4	0.266
Frequency of subpopulations																
T-cell subset																
T-cell	CD3+/CD45 + cells (%)	44.3	±	6.3	43.5	±	1.8	0.850	41.6	±	1.7	0.536	48.3	±	4.6	0.433
CD4 T	CD4+/CD3 + CD45 + cells (%)	7.33	±	3.6	14.9	±	3.2	0.054	12.2	±	1.2	0.133	13.2	±	1.6	0.089
CD8 T	CD8+/CD3 + CD45 + cells (%)	2.65	±	0.65	2.52	±	1.1	0.872	1.52	±	0.42	0.076	2.67	±	1.2	0.978
CD4 T subset																
	CD44 + CD62L+/CD4+ (%)	15.8	±	5.6	36.3	±	5.1	**0.009**	38.9	±	8.1	**0.019**	28.2	±	2.7	**0.042**
CM	CD127+/CD44 + CD62L+/CD4+ (%)	1.08	±	1.9	3.04	±	2.9	0.394	N E				2.19	±	2.5	0.575
effector T	CD44 + CD62L-/CD4+ (%)	30	±	1.5	31.2	±	6.8	0.797	32.2	±	8.6	0.706	37.5	±	4.7	0.096
CD8 T subset																
	CD44 + CD62L+/CD8+ (%)	13.8	±	8.2	23.4	±	9.9	0.266	27.3	±	15.3	0.270	14.1	±	3.2	0.952
effector T	CD44 + CD62L-/CD8+ (%)	20.1	±	10.2	15.8	±	5.8	0.566	17.6	±	0.3	0.709	31.1	±	3.1	0.199
naïve	CD44- CD62L+/CD8+ (%)	2.17	±	0.4	2.9	±	1.6	0.504	0.72	±	1.25	0.176	N E			
Exhausted T-cell																
	LAG3 + PD-1+/CD8+ (%)	9.04	±	1.8	9.47	±	1.7	0.776	15.6	±	2.4	**0.021**	15.9	±	8.5	0.292
	CD39 + PD-1+/CD8+ (%)	36.8	±	8.4	34.3	±	17.1	0.835	35.5	±	4.1	0.825	38.3	±	9.8	0.857
	TIM3 + PD-1+/CD8+ (%)	15.4	±	2.6	17.9	±	7.8	0.638	22.6	±	6.4	0.181	25.1	±	4.6	**0.048**
Myeloid cell																
	CD11b+ (%)	13.4	±	5.2	16.4	±	2.3	0.436	9	±	0.99	0.275	13.4	±	1.2	0.977
DC	CD11c + MHC Class2+/CD11b+ (%)	3.06	±	1.4	4.26	±	0.7	0.269	5.34	±	0.69	0.082	3.78	±	1.4	0.563
MDSC	Gr-1+/CD11c + MHC Class2+/CD11b+ (%)	8.9	±	4.7	10.2	±	9.8	0.849	3.27	±	1.5	0.164	5.93	±	3.2	0.423
Macrophage	F4_80+/CD11b+ (%)	5.59	±	2.5	18	±	1.5	**0.004**	20.9	±	8.2	0.073	12.3	±	1.1	**0.029**
Regulatory T																

Tumors were harvested from the control and DC-vaccinated groups. Each value represents the mean ± standard deviation from three mice. Ave.: average, SD standard deviation, DC: dendritic cell. NE: not evaluated. Bold values indicate statistical significance ($P < 0.05$), as determined using an unpaired two-tailed *t*-test.

	Cell populations	Control			DC				DC/aPD-1 Ab				aPD-1 Ab			
	CD25+/CD4+ (%)	17.8	±	7.1	18	±	5.2	0.975	6.83	±	1.5	0.107	12.5	±	2.5	0.317
Treg	GARP + FR4+/CD25+/CD4+ (%)	87.8	±	5.7	82.5	±	4.8	0.280	83.9	±	4.5	0.400	81.7	±	6.1	0.272
B cell	CD19+/CD3- (%)	1.66	±	1.2	3.63	±	1.9	0.225	1.51	±	0.08	0.860	1.88	±	0.4	0.787
NK	NK1.1+/CD3- (%)	0.14	±	0.08	0.06	±	0.02	0.215	0.07	±	0.08	0.343	0.24	±	0.06	0.175
Cell# of subpopulations																
	CD3+/CD45 + cell# (×105/g)	37	±	5.2	11.8	±	13.5	0.069	32	±	47.6	0.454	25.8	±	35.5	0.627
	CD4+/CD3 + CD45 + cell#(×105/g)	2.6	±	0.9	2.51	±	1.9	0.948	4.65	±	5.5	0.463	4.45	±	3.9	0.494
	CD8+/CD3 + CD45 + cell#(×105/g)	0.96	±	0.1	0.69	±	0.23	0.167	0.82	±	0.46	0.611	1.22	±	0.39	0.104

Tumors were harvested from the control and DC-vaccinated groups. Each value represents the mean ± standard deviation from three mice. Ave.: average, SD standard deviation, DC: dendritic cell. NE: not evaluated. Bold values indicate statistical significance ($P < 0.05$), as determined using an unpaired two-tailed *t*-test.

Table 3
Flow cytometry analysis of spleens from DC-vaccinated mice bearing EMT-6 tumors

	Cell populations	Control			DC				DC/aPD-1 Ab				aPD-1 Ab			
Separation data		Ave.		SD	Ave.		SD	p value	Ave.		SD	p value	Ave.		SD	p value
	Spleen weight(g)	0.2	±	0.02	0.3	±	0.1	0.069	0.4	±	0.1	**0.050**	0.4	±	0.1	0.073
	Collected cells (×10^6)	46.8	±	8.2	102.2	±	19.0	**0.024**	101.9	±	13.8	**0.008**	83.6	±	53.4	0.354
	CD45+/Total living cells (%)	99.2	±	0.2	98.7	±	0.3	0.072	98.2	±	0.2	**0.003**	98.1	±	0.9	0.161
Frequency of subpopulations																
Base population: Living cell/target population																
T-cell subset																
T-cell	CD3 + CD45 + cells (%)	34.2	±	2.8	23.5	±	2.5	**0.008**	20.4	±	4.1	**0.011**	18.6	±	2.0	**0.002**
CD4 T	CD4+/CD3 + CD45 + cells (%)	62.2	±	0.8	60.7	±	1.1	0.124	63.1	±	1.0	0.280	61.5	±	2.1	0.616
CD8 T	CD8+/CD3 + CD45 + cells (%)	29.4	±	0.4	28.7	±	2.3	0.688	28.2	±	1.0	0.170	29.3	±	1.7	0.976
Cell# of subpopulations																
	CD3+/CD45 + cell# (×10^6/g)	678.2	±	110.4	584.9	±	181.0	0.497	392.1	±	66.8	**0.007**	312.5	±	153.3	0.362
	CD4+/CD3 + CD45 + cell# (×10^6/g)	421.7	±	64.7	354.8	±	108.4	0.421	247.8	±	38.6	**0.008**	190.1	±	88.9	0.294
	CD8+/CD3 + CD45 + cell# (×10^6/g)	198.9	±	29.5	166.2	±	46.4	0.372	111.2	±	21.2	**0.013**	93.3	±	49.2	0.476

Spleens were harvested from both the control and DC-vaccinated groups. Various cell populations derived from human $CD45^+$ cells were measured using flow cytometry. Each value represents the mean ± standard deviation from three mice. Ave.: average, SD: standard deviation, DC: dendritic cell. Bold values indicate statistical significance ($P < 0.05$), as determined using an unpaired two-tailed *t*-test.

Profiling of mouse chemokine and cytokine gene expression in TILs via real-time PCR

Real-time PCR analysis revealed elevated expression of genes associated with mouse Th1 responses and effector T-cell activation, such as *CD3Z, CD8B, CSF1, CD19, CXCL10, IFNG*, and *IL12A*, in the DC-treated group compared with those in the control group (Supplementary Fig. 3). The addition of the anti-PD-1 antibody further elevated the expression levels of *CCR4, CCR6, CSF1*, and *CXCL10*.

Discussion

Advanced-stage TNBCs remain difficult to treat effectively. Chemotherapy specific for TNBCs has shown only a marginal effect on overall survival, despite the development of combination therapies involving intensive chemotherapy and ICIs [19, 20]. Recent neoadjuvant regimens incorporating ICI combination treatment have shown encouraging efficacy in early-stage TNBCs [10, 11]. However, the development of effective and safe therapeutic regimens for advanced disease remain an urgent clinical priority.

In recent years, our laboratory has focused on developing a novel reconstructive surgery-based immunotherapy termed "immune-flap," a skin-flap-mediated immunotherapeutic device. Over a decade of research has culminated in the successful establishment of an immune-flap-based immunotherapy approach to mitigate cancer recurrence in a rat model [12], where DC-injected immune flaps elicited effective antitumor responses against head and neck cancers.

Patients with advanced breast cancer are expected to benefit from reconstructive surgical techniques, including breast reconstruction using vascularized skin-flap transplantation [21, 22]. In the present study, we established a mouse immune-flap model using a mouse breast cancer cell line, EMT6, a well-characterized TNBC cell line expressing positive PD-L1 and moderate sensitivity to ICI treatment, [23–26] rendering them a widely used model for *in vivo* immunotherapy research.

In the present study, DC-injected skin flaps functioned as effective immunotherapeutic devices, exhibiting antitumor activity by increasing the number of TILs within the tumors, as observed through IHC analysis. Two immunotherapy regimens were established: DC vaccines alone, and a combination of DC vaccines and anti-PD-1 antibodies. TIL profiling revealed distinct patterns between these two treatments. DC vaccination mainly increased $CD4^+$ T cells, whereas the anti-PD-1 antibody alone stimulated the proliferation of $CD8^+$ effector T cells. Notably, the combination treatment resulted in a diminished antitumor effect, with a substantial reduction in TIL abundance within the tumors compared with those observed with either regimen alone. No synergistic or additive antitumor effects were observed in the combination therapy group. Potential immunological mechanisms underlying this immunosuppressive effect may include that the combination of both reagents may hinder their individual immunological effects, possibly through the modulating action of anti-PD-1 antibody on $PD\text{-}1^+$-activated $CD4^+$ T cells [27]. Another potential mechanism could contribute to such a suppressive effect, suggesting the need for the development of a better sequential regimen rather than concurrent therapy, as indicated by the failure of the concurrent regimen [28, 29].

Regarding the pattern of combination therapy, both concurrent and sequential strategies, such as DC followed by ICI, have been widely explored, with various ICIs, including antibodies against PD-1, PD-L1, and CTLA-4, trialed in early clinical studies [30–33]. A majority of these studies reported moderate synergistic or additive antitumor effects, including prolonged relapse-free periods, but without evident immunosuppressive effects in the combination modalities. Notably, our group observed a similar phenomenon in an *in vivo* study, in which the concurrent combination of a STAT3 inhibitor, which showed antitumor activity and remarkable T-cell infiltration against pancreatic tumors, and an anti-PD-1 antibody led to a remarkable reduction in antitumor efficacy and TIL recruitment [27]. These results suggest that the combination strategy may inhibit the individual effects of each treatment, resulting in unexpected attenuation of the antitumor effect, which appears to be a rare outcome in the context of combination with ICIs.

DC vaccination tended to increase the $CD19^+$ B cell population, whereas anti-PD-1 antibody treatment did not. The activation and maturation of B cells, which promote tumor-specific antibody production, may be triggered by activated CD4 helper T cells induced by DC vaccination [34–36]. These results suggest that the increase in B cell numbers is likely a specific effect of DC vaccination, rather than a result of anti-PD-1 antibody treatment.

Although our results are promising, some technical challenges and limitations need to be addressed before the current protocol can be translated into clinical practice. Despite these limitations, this study demonstrated that the DC vaccine-injected immune flap functioned as an effective immunotherapeutic device, promoting efficient migration to the regional lymph nodes within the flap and enhancing TIL recruitment within the tumors. However, the identification and development of an optimal regimen for combining DC vaccination and ICI therapy warrant further research.

Declarations

Financial Disclosure Statement

This work was supported by JSPS KAKENHI (grant number 21K09785).

Conflict of interest

The authors declare that they have no conflicts of interest.

Author Contribution

Yoshitaka Haga designed the study, drafted the manuscript, and conducted part of the in vivo experiments. Tadashi Ashizawa and Akari Kanematsu performed the in vivo experiments and completed the animal studies. Chie Maeda and Akira Iizuka performed the FACS analysis of TILs. Tomoatsu Ikeya performed in vitro immunological experiments. Takashi Sugino assisted with TIL analysis using IHC. Hiroki Mori monitored the experimental progress, provided advice, and coordinated the scheduling of experiments. Yasuto Akiyama and Jun Araki supervised the research project and were responsible for completing the study. All authors read and approved the final draft of the manuscript.

Acknowledgement

The authors thank Dr. Koji Maruyama for his assistance in maintaining the tumor-bearing mice in the animal facility. Additionally, we thank Dr. Haruo Miyata, Dr. Kazue Yamashita, Dr. Yoshichika Yasunaga, and Dr. Ken Yamaguchi for their technical assistance.

Data Availability

All data generated or analyzed during this study are included in this published article (and its Supplementary Information file).

References

1. Aebi S, Karlsson P, Wapnir IL (2022) Locally advanced breast cancer. Breast 62(suppl 1):S58–S62
2. Dhanushkodi M, Sridevi V, Shanta V et al (2021) Locally advanced breast cancer (LABC): Real-world outcome of patients from cancer institute, Chennai. JCO Glob Oncol 7:767–781
3. Shigekawa T, Osaki A, Sekine H et al (2015) Safety and feasibility of adjuvant chemotherapy with S-1 in Japanese breast cancer patients after primary systemic chemotherapy: A feasibility study. BMC Cancer 15:253
4. Masuda N, Lee SJ, Ohtani S et al (2017) Adjuvant capecitabine for breast cancer after preoperative chemotherapy. N Engl J Med 376(22):2147–2159
5. Cortes J, Cescon DW, Rugo HS et al (2020) KEYNOTE-355 Investigators: Pembrolizumab plus chemotherapy versus placebo plus chemotherapy for previously untreated locally recurrent inoperable or metastatic triple-negative breast cancer (KEYNOTE-355): A randomized, placebo-controlled, double-blind, phase 3 clinical trial. Lancet 396(10265):1817–1828
6. Villacampa G, Tolosa P, Salvador F et al (2022) Addition of immune checkpoint inhibitors to chemotherapy versus chemotherapy alone in first-line metastatic triple-negative breast cancer: A systematic review and meta-analysis. Cancer Treat Rev 104:102352
7. Wakelee H, Liberman M, Kato T et al (2023) Perioperative pembrolizumab for early-stage non-small-cell lung cancer. N Engl J Med 389(6):491–503
8. Amaria RN, Reddy SM, Tawbi HA et al (2018) Neoadjuvant immune checkpoint blockade in high-risk resectable melanoma. Nat Med 24(11):1649–1654
9. Chalabi M, Fanchi LF, Dijkstra KK et al (2020) Neoadjuvant immunotherapy leads to pathological responses in MMR-proficient and MMR-deficient early-stage colon cancers. Nat Med 26(4):566–576
10. Schmid P, Cortes J, Pusztai L et al (2020) Pembrolizumab for early triple-negative breast cancer. N Engl J Med 382(9):810–821
11. Nederlof I, Isaeva OI, de Graaf M et al (2024) Neoadjuvant nivolumab or nivolumab plus ipilimumab in early-stage triple-negative breast cancer: a phase 2 adaptive trial. Nat Med 30(11):3223–3235
12. Inoue K, Saegusa N, Omiya M et al (2015) Immunologically augmented skin flap as a novel dendritic cell vaccine against head and neck cancer in a rat model. Cancer Sci 106(2):143–150
13. Rockwell SC, Kallman RF, Fajardo LF (1972) Characteristics of a serially transplanted mouse mammary tumor and its tissue-culture-adapted derivative. J Natl Cancer Inst 49(3):735–749
14. Kresl JJ, Potempa LA, Anderson B, Radosevich JA (1999) Inhibition of a mouse mammary adenocarcinoma (EMT6) growth and metastases in mice by a modified form of C-reactive protein. Tumour Biol 20(2):72–87
15. Percie du Sert N, Hurst V, Ahluwalia A et al (2020) The ARRIVE guidelines 2.0: Updated guidelines for reporting animal research. Plos Biol 18(7):e3000410
16. Akiyama Y, Ashizawa T, Iizuka A et al (2022) Development of novel small antitumor compounds inhibiting PD-1/PD-L1 binding. Anticancer Res 42(11):5233–5247
17. Akiyama Y, Watanabe M, Maruyama K, Ruscetti FW, Wiltrout RH, Yamaguchi K (2000) Enhancement of antitumor immunity against B16 melanoma tumor using genetically modified dendritic cells to produce cytokines. Gene Ther 7(24):2113–2121
18. Miyata H, Akiyama Y, Iizuka A et al (2022) Development of an automatic measurement method for CD8 and PD-1 positive T cells using image analysis software. Anticancer Res 42(1):419–427
19. Ji Q, Ding J, Hao M, Luo N, Huang J, Zhang W (2021) Immune checkpoint inhibitors combined with chemotherapy compared with chemotherapy alone for triple-negative breast cancer: a systematic review and meta-analysis. Front Oncol 11:795650
20. Brown LC, Loi S (2022) Immune checkpoint inhibition in the treatment of early stage triple negative breast cancer: 2021 update. Breast 62(suppl 1):S29–S33
21. Myckatyn TM, Wagner IJ, Mehrara BJ et al (2017) Cancer risk after fat transfer: A multicenter case-cohort study. Plast Reconstr Surg 139(1):11–18
22. Tomita K, Kubo T (2023) Recent advances in surgical techniques for breast reconstruction. Int J Clin Oncol 28(7):841–846

23. Jiao S, Xia W, Yamaguchi H et al (2017) PARP inhibitor upregulates PD-L1 expression and enhances cancer-associated immunosuppression. Clin Cancer Res 23(14):3711–3720
24. Xu C, Zhang Y, Rolfe PA et al (2017) Combination therapy with NHS-muIL12 and avelumab (anti-PD-L1) enhances antitumor efficacy in preclinical cancer models. Clin Cancer Res 23(19):5869–5880
25. Mariathasan S, Turley SJ, Nickles D et al (2018) TGFβ attenuates tumour response to PD-L1 blockade by contributing to exclusion of T cells. Nature 554(7693):544–548
26. Sham NFR, Hasani NAH, Hasan N et al (2023) Acquired radioresistance in EMT6 mouse mammary carcinoma cell line is mediated by CTLA-4 and PD-1 through JAK/STAT/PI3K pathway. Sci Rep 13(1):3108
27. Ashizawa T, Iizuka A, Maeda C et al (2019) Impact of combination therapy with anti-PD-1 blockade and a STAT3 inhibitor on the tumor-infiltrating lymphocyte status. Immunol Lett 216:43–50
28. Calmeiro J, Carrascal MA, Tavares AR et al (2021) Pharmacological combination of nivolumab with dendritic cell vaccines in cancer immunotherapy: an overview. Pharmacol Res 164:105309
29. Zanotta S, Galati D, De Filippi R, Pinto A (2024) Enhancing dendritic cell cancer vaccination: the synergy of immune checkpoint inhibitors in combined therapies. Int J Mol Sci 25(14):7509
30. Kyr M, Mudry P, Polaskova K et al (2024) Personalized dendritic cell vaccine in multimodal individualized combination therapy improves survival in high-risk pediatric cancer patients. Int J Cancer 155(8):1443–1454
31. Salewski I, Kuntoff S, Kuemmel A et al (2021) Combined vaccine-immune-checkpoint inhibition constitutes a promising strategy for treatment of dMMR tumors. Cancer Immunol Immunother 70(12):3405–3419
32. Fan T, Zhang M, Yang J, Zhu Z, Cao W, Dong C (2023) Therapeutic cancer vaccines: advancements, challenges, and prospects. Signal Transduct Target Ther 8(1):450
33. Guo Z, Yuan Y, Chen C et al (2022) Durable complete response to neoantigen-loaded dendritic-cell vaccine following anti-PD-1 therapy in metastatic gastric cancer. NPJ Precis Oncol 6(1):34
34. Goc J, Germain C, Vo-Bourgais TKD et al (2014) Dendritic cells in tumor-associated tertiary lymphoid structures signal a Th1 cytotoxic immune contexture and license the positive prognostic value of infiltrating $CD8^+$ T cells. Cancer Res 74(3):705–715
35. Germain C, Gnjatic S, Tamzalit F et al (2014) Presence of B cells in tertiary lymphoid structures is associated with a protective immunity in patients with lung cancer. Am J Respir Crit Care Med 189(7):832–844
36. Heath WR, Kato Y, Steiner TM, Caminschi I (2019) Antigen presentation by dendritic cells for B cell activation. Curr Opin Immunol 58:44–52

Figures

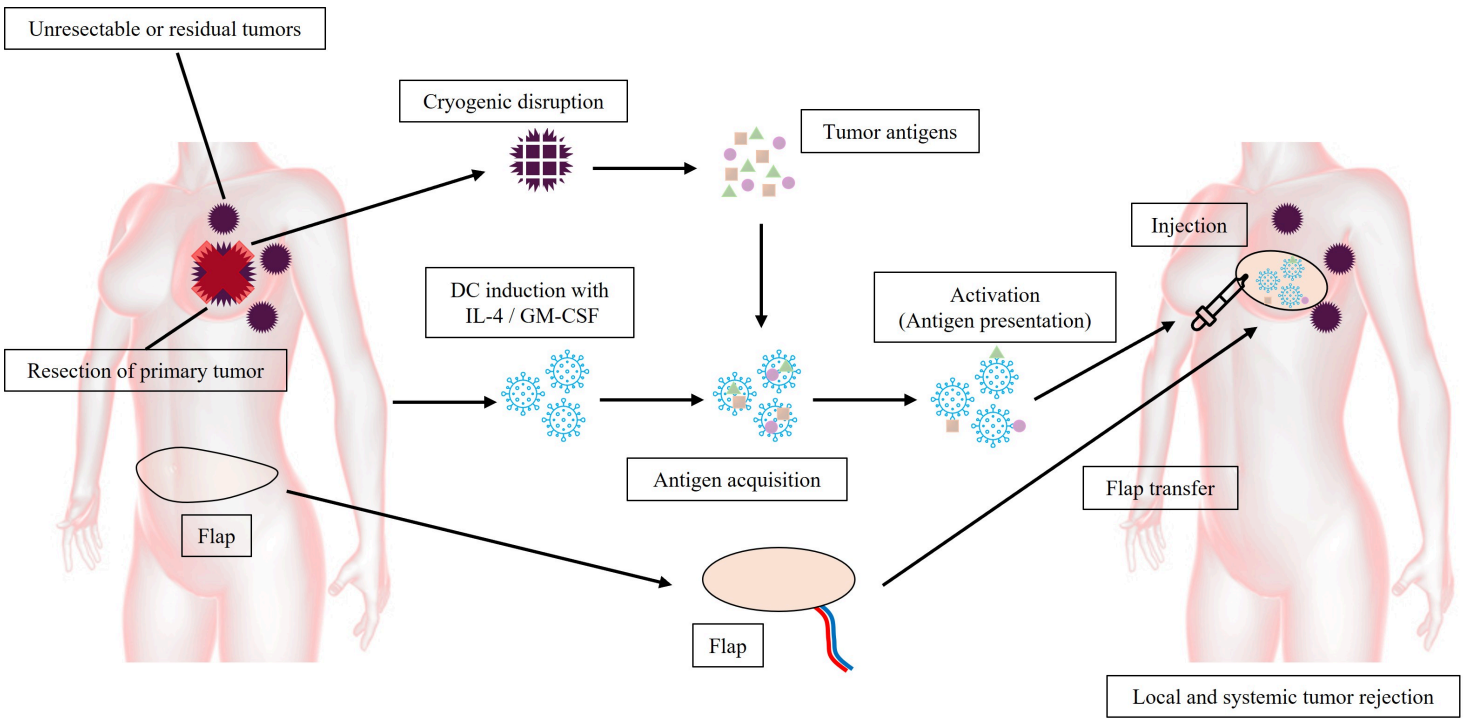


Figure 1

Local immunotherapy for skin-flap graft followingbreast cancer resection.

Dendritic cells (DCs) were cultured and stimulated with antigens derived from the resected tumors. The antigen-stimulated DCs were injected into the transplanted skin flap, which was used for reconstruction after breast cancer resection, to provide localized control against tumor recurrence and residual tumors.

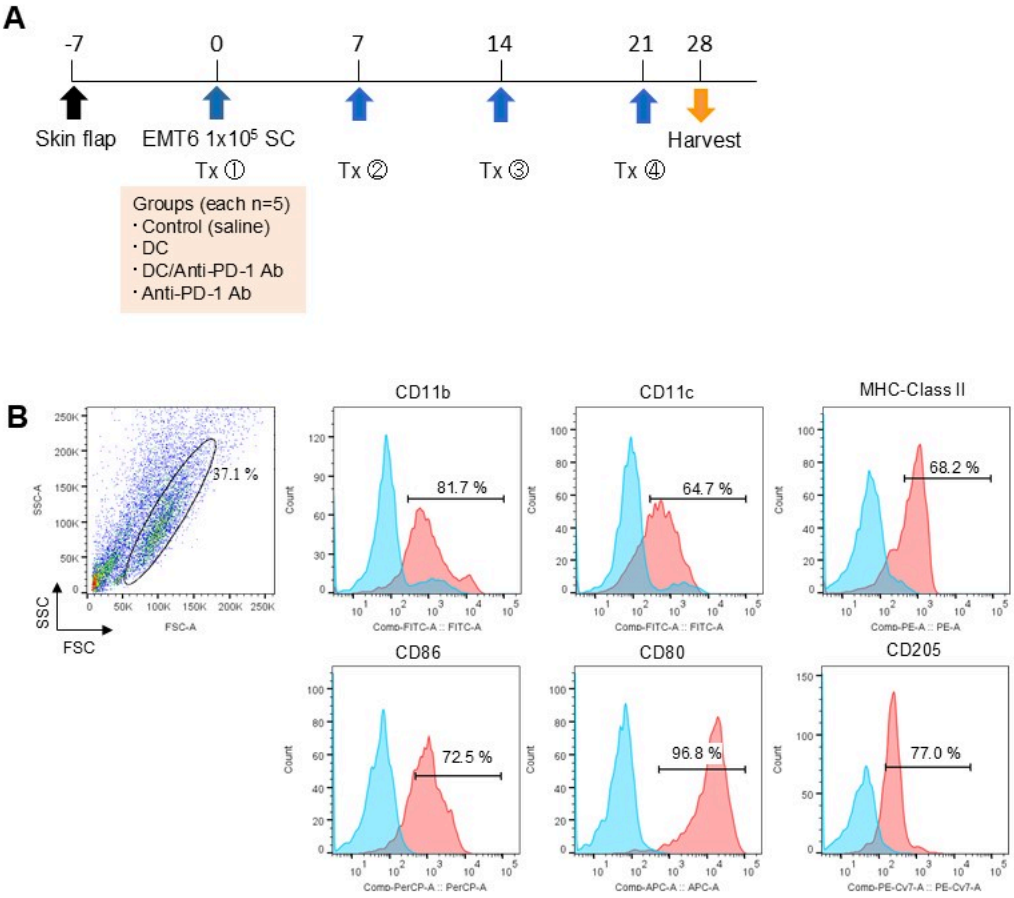


Figure 2

In vivo experimental protocol and characterization of mouse bone marrow-derived DCs.

(A) Experimental schedule for the *in vivo* immuno-flap-based DC vaccination model targeting EMT6 tumors. Cultured DCs were injected subcutaneously into the skin flap at four weekly intervals. Tumors and spleens were harvested on day 28 for analysis. (B) Flow cytometric characterization of mouse bone marrow-derived DCs. The expression of DC-specific markers (CD11b, CD11c, CD80, CD86, CD205, and MHC class II) is depicted in histograms.

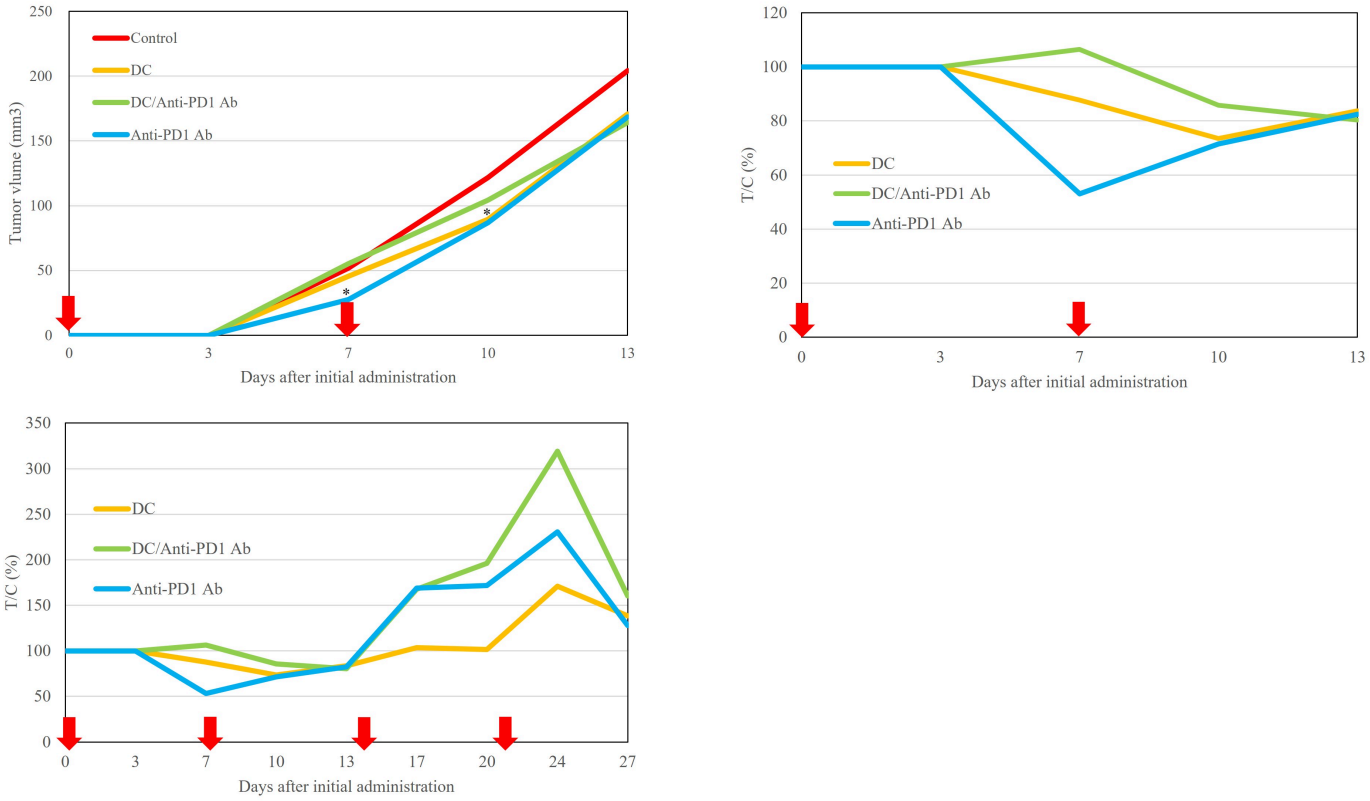


Figure 3

Effect of immuno-flap-based DC vaccination on EMT6 tumor growth.

Four cohorts were established: control (physiological saline alone), DC vaccine alone, anti-PD-1 antibody alone, and a combination of the DC vaccine with anti-PD-1 antibody. Each groupcomprised five mice. (A) Short-term DC vaccination experiment. DC vaccine was administered twice, on days 0 and 7. The actual tumor volumes and tumor volume ratio (T/C:test group/control group) are shown. *: On day 7, control vs. anti-PD-1 Ab; *P*= 0.0070. *: On day 9, control vs. DC; *P* = 0.0379. (B) Long-term DC vaccination experiment. DC vaccine was administered four times on days 0, 7, 14, and 21. *Statistically significant, *P* < 0.05. Each cohort comprised five tumor-bearing mice.

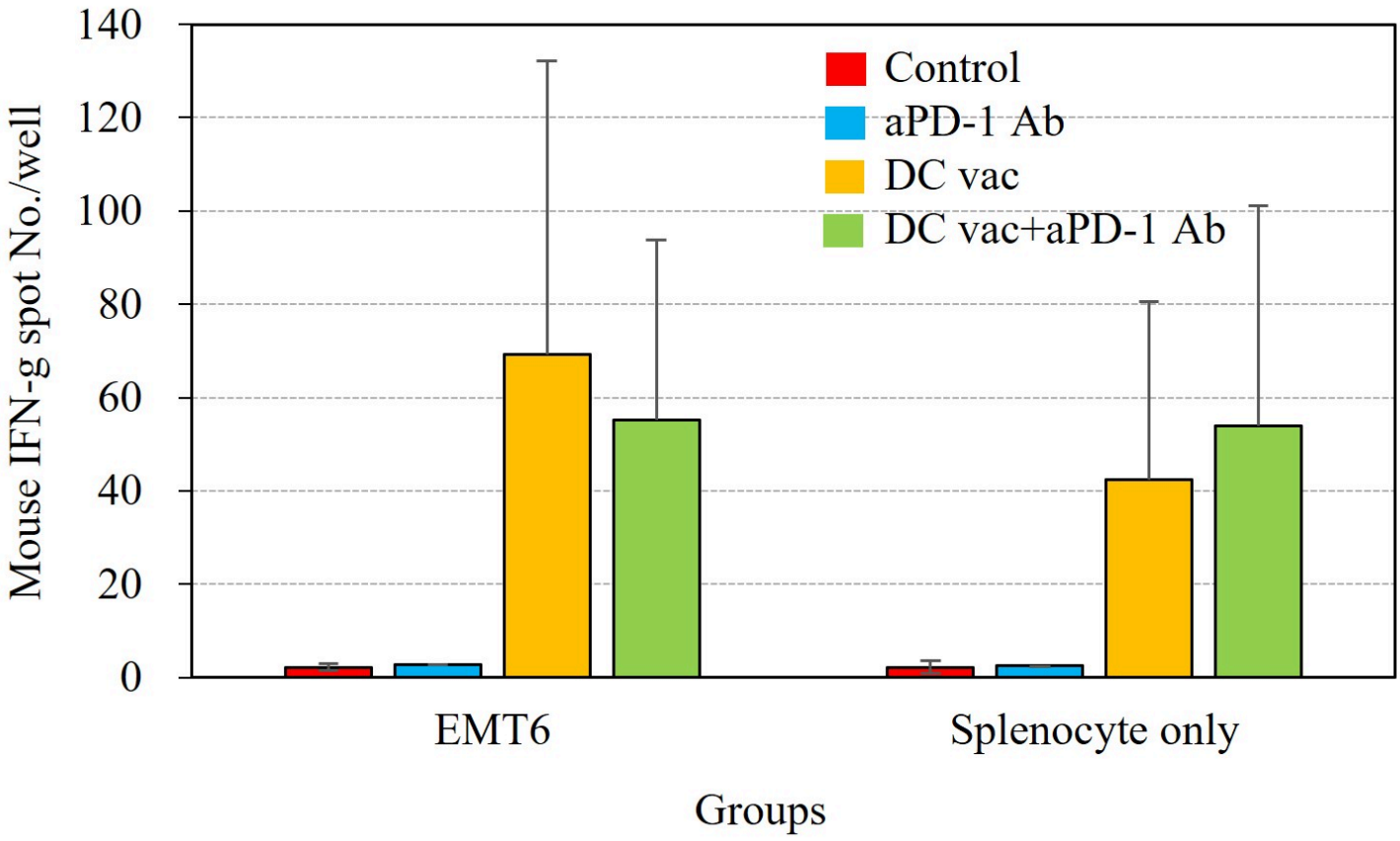


Figure 4

Characterization of CTLs from spleen cells using ELISPOT assay.

The number of IFN-γ spots per well was compared among the four cohorts (control, DC vaccine alone, anti-PD-1 antibody alone, and combination of DC vaccine with anti-PD-1 antibody) using 1×10^5 spleen cells. EMT6 tumor cells (1×10^5 cells/well) were added as target cells and incubated with effector cells. EMT6: number of spots after EMT6 activation; splenocyte only: number of spots without EMT6 activation. Each column represents the mean values of three mice.

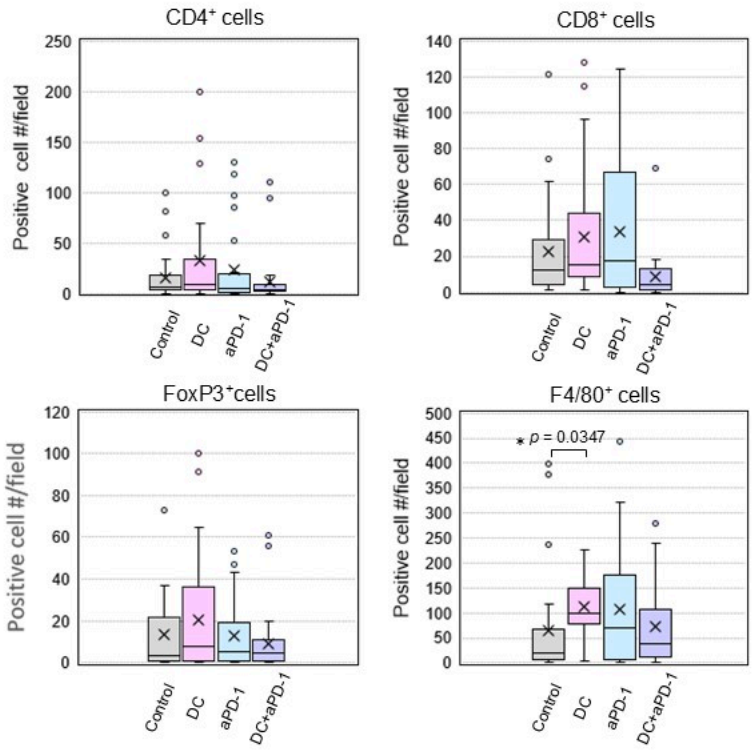


Figure 5

Measurement of tumor-infiltrating immune cells using immunohistochemistry and image analysis software. Tumor sections were stained with various antibodies, including anti-CD4, anti-CD8, and anti-FoxP3 antibodies against T cells and anti-F4/80 antibody against macrophages. Five high-magnification fields (×200) were selected from each tumor section, and the number of positive cells was quantified using image analysis software. The mean number of positive cells per field is shown in columns. In the F4/80$^+$ cell panel, a significant difference was observed between the control and DC groups (P = 0.0347). *Statistically significant, P < 0.05. Each column represents the mean value of formalin-fixed paraffin-embedded specimens derived from three mice.

Supplementary Files

This is a list of supplementary files associated with this preprint. Click to download.

- FigureSupplementalDigitalContent1revise20251123.jpg
- FigureSupplementalDigitalContent3revise20251123.jpg
- FigureSupplementalDigitalContent2033025.jpg